# Contributions to sea level variability along the Norwegian coast for 1960–2010

K. Richter,[1,2] J. E. Ø. Nilsen,[2,3] and H. Drange[1,2,4]

Received 13 December 2011; revised 20 April 2012; accepted 25 April 2012; published 26 May 2012.

[1] Global sea level has been rising by about 20 cm during the last century and is expected to continue to rise in the 21st century. The rise and variability is not spatially uniform. To be able to project local changes in relative sea level (RSL), it is important to identify the processes that govern regional RSL variability. In this study, we assess the importance of different contributions to RSL variability along the coast of Norway in the period 1960–2010. By using hydrographic station data at the coast, sea level pressure, and observed vertical land uplift, we compute RSL changes due to thermal expansion, haline contraction, the inverted barometer effect, and land uplift caused by glacial isostatic adjustment. The combination of these contributions is compared to RSL variability observed with tide gauges. For all but the two southernmost stations, the reconstructed RSL explains 70–85% of the observed variability of the monthly sampled time series. The inverted barometer effect is responsible for more than half of the explained variability, while thermosteric height represents the largest contribution to the linear trend. Due to land uplift, the local RSL rise is weaker and partly negative along the Norwegian coast. The residual (observed minus reconstructed) shows a positive trend ranging from 1.3 mm $yr^{-1}$ to 2.3 mm $yr^{-1}$. It is speculated that the reason for this is an increase of mass in the ocean due to melting of land-based ice and, to a lesser degree, the combined thermohaline expansion in the deep Nordic seas.

**Citation:** Richter, K., J. E. Ø. Nilsen, and H. Drange (2012), Contributions to sea level variability along the Norwegian coast for 1960–2010, *J. Geophys. Res.*, *117*, C05038, doi:10.1029/2011JC007826.

## 1. Introduction

[2] Data from tide gauges indicate that the global sea level has been rising by about 25 cm since the start of the observational record in 1860 [*Church and White*, 2011; *Woodworth et al.*, 2011a]. Sea level rise since 1992, inferred from satellite-borne altimeters, shows an increase of slightly more than 3 mm $yr^{-1}$ [*Cazenave and Llovel*, 2010]. The two independent time series are in general agreement during the overlapping period [*Woodworth et al.*, 2011a]. It is therefore a well-established fact that the global sea level is rising. Whether the rise of the observed sea level is accelerating, which is a key question related to projections of future sea level rise and its consequences for coastal regions, depends heavily on the time span of the analysis. Based on a reconstructed sea level time series, both *Jevrejeva et al.* [2006] and *Woodworth et al.* [2011b] indicate an accelerated sea level rise starting at the end of the 19th century.

[3] A main element of the rising sea level is the enhanced uptake of heat by the ocean and the subsequent thermal expansion of the water masses. Other major contributions are the melting of land-based glaciers and the large ice sheets on Greenland and Antarctica. According to the Fourth Assessment Report (AR4) of the Intergovernmental Panel on Climate Change (IPCC), thermal expansion contributed with about 40% while glaciers and ice sheets accounted for the remaining 40% and 20%, respectively, for the period 1961–2003 [*Meehl et al.*, 2007]. It is, however, only in recent years with improved observation platforms that the major contributing factors to the global sea level form a near closed budget [*Cazenave et al.*, 2008; *Leuliette and Miller*, 2009].

[4] Recent analyses show that the relative importance of the individual contributions to the global sea level is subject to large temporal variations. Synthesis studies by *Cazenave et al.* [2008] and *Cazenave and Llovel* [2010] suggest that the importance of melting ice sheets to the total sea level rise increased to 40% during the period 2003–2007/2008, whereas the contribution from thermal expansion decreased to about 15%. The increasing contribution from melting ice sheets is in general agreement with the reported acceleration of the melting of land-based ice [*Rignot et al.*, 2011].

[5] Sea level is not rising at the same rate globally but exhibits significant spatial variations [*Church et al.*, 2004; *Cazenave et al.*, 2008] in addition to the large interannual and decadal fluctuations superimposed on the long-term

[1]Geophysical Institute, University of Bergen, Bergen, Norway.
[2]Bjerknes Center for Climate Research, Bergen, Norway.
[3]Nansen Environmental and Remote Sensing Center, Bergen, Norway.
[4]Uni Research AS, Bergen, Norway.

Corresponding author: K. Richter, Geophysical Institute, University of Bergen, Allégaten 70, N-5007 Bergen, Norway. (kristin.richter@gfi.uib.no)


0148-0227/12/2011JC007826

increasing trend [*Jevrejeva et al.*, 2006]. Several studies have examined local changes in the observed, and to some extent in the modeled, sea level. Examples of regional sea level analysis cover the Arctic Ocean [*Pavlov*, 2001; *Proshutinsky et al.*, 2001, 2004, 2007], the North Atlantic Ocean [*Llovel et al.*, 2011], the coast of Scotland [*Rennie and Hansom*, 2011], the German Bight [*Wahl et al.*, 2011], the Mediterranean Sea [*García-García et al.*, 2010; *Meyssignac et al.*, 2011], and the coast of the U.S.A. [*Yin et al.*, 2009; *Weiss et al.*, 2011]. Recent regional sea level studies deduced from global analysis are given by, e.g., *Riva et al.* [2010], *Yin et al.* [2010], *Pardaens et al.* [2011], *Marcos et al.* [2011] and *Slangen et al.* [2011].

[6] The objective of this study is to quantify, to the extent possible, the major contributions to the observed sea level changes, in terms of variability and trends, along the eastern rim of the Nordic seas during the past 50 years. While the steric height anomaly is globally mostly accounted for by thermal expansion, haline contraction is almost equally important in the subpolar North Atlantic. Here, cooling and simultaneous freshening lead to density compensated linear trends in steric height during the second half of the 20th century [*Antonov et al.*, 2002; *Levitus et al.*, 2005; *Steele and Ermold*, 2007; *Siegismund et al.*, 2007]. It is however not clear to what extent changes in sea surface height in the interior of the Nordic seas are relevant for changes in sea level along the Norwegian coast. The coastal water is, for instance, influenced by both relatively warm Atlantic Water and fresh water from land runoff, whereas the interior of the basin mainly consists of cold and relatively fresh water of polar origin.

[7] The dominant mode of atmospheric variability over the Nordic seas is characterized by a meridional pressure gradient and southwesterly winds, commonly represented by the North Atlantic Oscillation (NAO) index [*Hurrell*, 1995]. The effect of atmospheric forcing on sea level along the Norwegian coast is dual. Changes in surface pressure affect sea surface height through the inverted barometer effect (IBE) while the prevailing southwesterly winds push the water onshore. Storm surges combine both effects and may lead to exceptionally high sea levels along the northwestern European coast, impacting existing infrastructures.

[8] *Wakelin et al.* [2003] found good correlation between sea level observed along the western European coast and the NAO index. In particular, wind effects appeared to dominate over IBE in the southeastern North Sea while the wind contribution away from the shelf was negligible. *Jevrejeva et al.* [2005] demonstrated that the link between NAO and European winter sea level persisted only for selective time intervals, probably due to a meridional shift in westerlies that is not properly represented by a static NAO index. This finding strongly indicates cautious use of the NAO index as a time invariant proxy for winter variations in the sea level in the region.

[9] Fennoscandinavia experiences relatively large, but spatially nonuniform, glacial isostatic uplift [*Ekman*, 1996; *Milne et al.*, 2001]. Recent estimates of the uplift rates are given by *Vestøl* [2006], varying from more than 40 cm per century in the inner Oslo fjord in southeast Norway to about 10 cm per century along the outermost part of southern and western Norway. Consequently, and particularly on multidecadal and longer time scales, changes in sea level with respect to land do not necessarily reflect changes in sea level in the open ocean. In this study, we investigate changes in the *relative sea level* (RSL), that is changes in the sea level with respect to land. For sea level estimates representing the open ocean, we use the term *sea surface height* (SSH).

[10] Among other, less directly observable contributions to local RSL change are redistribution of ocean mass onto continental shelves due to deep ocean expansion, and the expectedly important mass input from glaciers and ice caps. These contributions will be roughly estimated and briefly discussed in light of the observed RSL variability and trends.

[11] The main objective of the present study is to identify and quantify the contributions to the observed RSL variability along the Norwegian coast, and to assess to what degree RSL can be estimated from the contributions taken into account.

[12] In section 2 we describe the data and methods used to compute and analyze the contributions to RSL variability. Results are presented and observed RSL is compared to its reconstruction in section 3. The outcome and missing contributions are discussed in section 4 and the study is concluded in section 5.

## 2. Data and Methods

[13] Various factors contribute to variations in RSL. In this study, we consider changes induced by atmospheric and thermohaline variability, as well as vertical land uplift. The combination of these contributions yields the reconstructed RSL,

$$\mathrm{RSL}_{rc} = \eta_p + \eta_T + \eta_S + \mathrm{GIA}, \tag{1}$$

which will be compared to the observed RSL. In the expression above, $\eta_p$ is the SSH variability due to surface pressure fluctuations (the IBE effect), $\eta_T$ and $\eta_S$ are the thermosteric and halosteric contributions, respectively, and GIA is a linear trend representing vertical land uplift due to glacial isostatic adjustment. Accordingly,

$$\mathrm{RSL} = \mathrm{RSL}_{rc} + \eta_{res}, \tag{2}$$

where $\eta_{res}$ is the sea level residual that is not explained by our reconstruction.

[14] In the following, we will describe the data we use to compute the single contributions, and how we quantify their relative importance on interannual time scales and with respect to trends.

### 2.1. Tide Gauge Data

[15] Observed RSL is obtained from the historical tide gauge data set compiled by the Permanent Service for Mean Sea Level (PSMSL) [*Woodworth and Player*, 2003] for the period 1960–2010. We use exclusively the Revised Local Reference data, presenting the sea level measured relative to a coastal benchmark at each station. Our criteria for selecting tide gauge time series are multidecadal records (>30 years) without large gaps (>1.5 years) covering the past 50 years (Figure 1 and Table 1). Longer records are available at some stations but for consistency and due to the limited availability of auxiliary data (see below), we confine our analysis to the period after 1960.

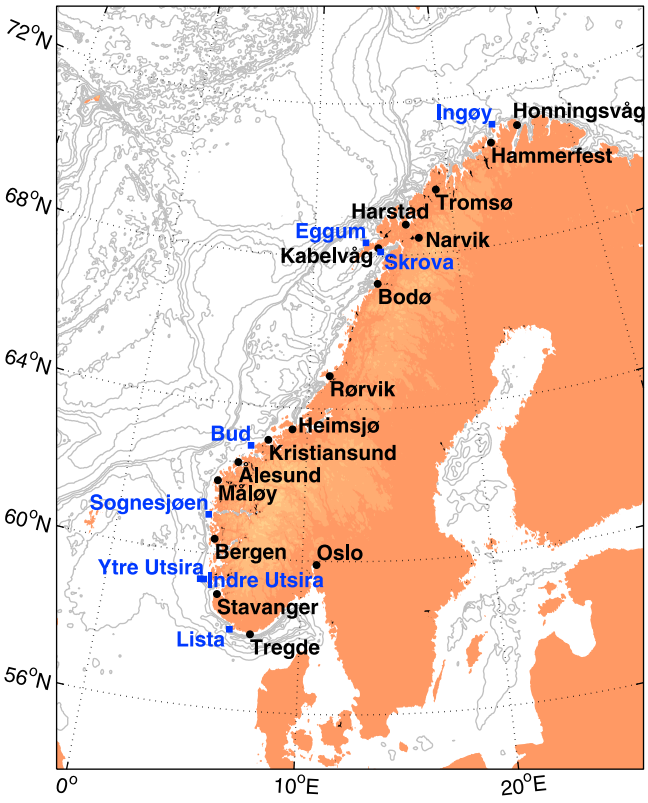


**Figure 1.** Positions of the tide gauges used in the analysis (black) and locations of the hydrographic stations (blue).

## 2.2. Vertical Land Movement

[16] The most important process contributing to vertical land movement in the northeastern North Atlantic is GIA (as opposed to earthquakes, increased groundwater extraction and deposits from river discharges). There are two approaches to determine vertical land uplifts related to GIA. The most common approach is by means of geodynamic modeling. The second approach is to use observations. *Vestøl* [2006] combined leveling, historical tide gauge recordings and global positioning system data to derive land uplift rates for Fennoscandinavia.

[17] Land uplift estimates as predicted by the ICE-5G models are supplied by the Permanent Service for Mean Sea Level [*Peltier*, 2004] for two different Earth models (VM2 and VM4). There are large discrepancies between the modeled estimates (not shown). Both are lower than the estimates from *Vestøl* [2006]. Peltiers model is global, so small-scale anomalies in Earths structure are not properly modeled.

[18] Therefore, we use the data set provided by *Vestøl* [2006]. It is partly based on tide gauges (from longer periods than discussed here) but we consider it the best available estimate of vertical land uplift rates to date. Rates of vertical uplift at the positions of the tide gauge stations are presented in Table 1.

[19] A problem here is that data coverage close to tide gauge stations is in general sparse. The reliability of the uplift rates varies geographically depending on the spatial density of tide gauges with long-term observations of sea level. Thus, uncertainties in the derived rates are not geographically uniform [*Vestøl*, 2006, Figure 7]. In this study, however, we use the average uncertainty of 0.5 mm $yr^{-1}$.

## 2.3. Thermohaline Contributions

[20] Hydrographic station data along the Norwegian coast were provided by the Institute of Marine Research (IMR), Bergen, Norway. There are eight permanent stations along the Norwegian coast (Figure 1) that have been maintained for several decades and provide vertical profiles of temperature and salinity. The frequency of measurements varies with time. Except for Skrova at 68°N with almost weekly sampling, each station has been sampled approximately twice a month, but with gaps in the data from one to several months. Data cover the period 1960–2010, with the exception of Ingøy (1968–2010) and Bud (1971–2010).

[21] Steric height along the coast is computed following *McClimans et al.* [1999]:

$$\eta_{st} = \int (\rho_0 - \rho)/\rho_0 \, dz, \tag{3}$$

**Table 1.** Tide Gauges With Monthly Observations of RSL Obtained From the PSMSL[a]

| Tide Gauge | Longitude | Latitude | Period | GIA (mm $yr^{-1}$) | IMR Station |
|---|---|---|---|---|---|
| Honningsvåg | 25.6 | 70.6 | 1970– | 2.1 | Ingøy |
| **Hammerfest** | 23.4 | 70.4 | 1957– | 2.5 | Ingøy |
| **Tromsø** | 18.6 | 69.4 | 1952– | 2.7 | Skrova |
| Harstad | 16.3 | 68.5 | 1952– | 2.7 | Skrova |
| Narvik | 17.2 | 68.3 | 1928–1940, 1947– | 4.4 | Skrova |
| Kabelvåg | 14.3 | 68.1 | 1948– | 2.6 | Skrova |
| Bodø | 14.2 | 67.2 | 1949– | 3.6 | Skrova |
| Rørvik | 11.2 | 64.5 | 1972– | 4.2 | Bud |
| Heimsjø | 9.1 | 63.3 | 1928– | 3.1 | Bud |
| **Kristiansund** | 7.5 | 63.1 | 1952– | 2.6 | Bud |
| Ålesund | 6.1 | 62.3 | 1945–1946, 1951– | 1.9 | Sognesjøen |
| Måløy | 5.1 | 61.6 | 1943– | 1.9 | Sognesjøen |
| **Bergen** | 5.2 | 60.2 | 1883–1889, 1928– | 1.7 | Sognesjøen |
| **Stavanger** | 5.4 | 58.6 | 1919–1939, 1946– | 1.2 | Indre Utsira |
| **Tregde** | 7.3 | 58.0 | 1927– | 1.3 | Lista |
| Oslo | 10.4 | 59.5 | 1885–1890, 1914– | 4.9 | Lista |

[a]The position of each tide gauge station and the availability of data is given. GIA is provided in the fifth column based on *Vestøl* [2006]. The last column shows the hydrographic station used to compute the thermohaline contributions for the selected tide gauges (see Figure 1). The stations in bold are discussed in section 3.2.

where the integration is from the bottom of the profile to the surface. The reference density $\rho_0$ is the mean of the vertical average of all profiles at the given station. Absolute steric height is very sensitive to the choice of $\rho_0$, while anomalies and linear trends are rather unaffected. According to *Gill and Niiler* [1973], $\eta_{st}$ can be divided into a thermal ($\eta_T$) and a haline ($\eta_S$) component assuming the deviations from a reference temperature and salinity are small. Accordingly,

$$\eta_T = \int \alpha(T^*, S^*)(T - T_0)\,\mathrm{d}z, \quad \eta_S = \int \beta(T^*, S^*)(S - S_0)\mathrm{d}z, \tag{4}$$

where $\alpha$ and $\beta$ are the thermal expansion and haline contraction coefficients of sea water, respectively [*McDougall*, 1987], evaluated at $T^* = (T + T_0)/2$ and $S^* = (S + S_0)/2$ following *Siegismund et al.* [2007]. Here, $T_0$ and $S_0$ are reference temperature and salinity, respectively.

[22] The locations of the hydrographic stations are not identical to the locations of tide gauges (Figure 1). Therefore, RSL observations from tide gauges have been paired with the steric height, computed from (3), based on their location and the highest correlation coefficients between steric height and RSL observed with tide gauges (not displayed). Table 1 shows which hydrographic station has been assigned to which tide gauge station. The hydrographic stations at Ytre Utsira and Indre Utsira, and at Skrova and Eggum are situated close to each other (Figure 1). Accordingly, from each pair only one station, namely Indre Utsira and Skrova respectively, has been used for the analysis.

### 2.4. Inverted Barometer Effect

[23] The SSH variability is strongly influenced by changes in atmospheric pressure through the inverted barometer effect (IBE). Generally, a 1 mbar increase in surface pressure produces a 1 cm depression of sea level. We use monthly atmospheric surface pressure from the National Centers for Environmental Prediction-National Center for Atmospheric Research (NCEP-NCAR) reanalysis [*Kalnay et al.*, 1996] at 2.5° spatial resolution to apply the inverted barometric correction

$$\eta_p = -\Delta p/(\rho_0 g). \tag{5}$$

Here $\Delta p$ is the pressure fluctuations leading to IBE, $\rho_0$ is the reference density of sea water taken as 1025 kg m$^{-3}$, and $g$ is the acceleration due to gravity. The pressure fluctuations are defined as the deviations from the mean over the period 1960–2010. The pressure is taken from the ocean grid point closest to the location of the tide gauge station.

### 2.5. Variability and Trends

[24] The focus of this study is to assess the contribution to the above mentioned components to the observed RSL variability and change. The analysis is based on monthly time series. Covariability is explored by means of correlation and covariance analysis. If not stated otherwise, the linear trend has been removed from all time series prior to computing correlation coefficients and covariances. Therefore, linear long-term trends are not included in the covariance analysis although they may contribute significantly to the variance on long time scales.

[25] For two time series $x$ and $y$, the correlation coefficient is computed using

$$r = \frac{\sum xy}{\sqrt{\sum x^2 \sum y^2}} = \frac{cov(x,y)}{\sqrt{var(x)var(y)}}. \tag{6}$$

The variance explained by $\mathrm{RSL}_{rc}$ in equation (2) is then

$$R^2 = 1 - \frac{var(\eta_{res})}{var(\mathrm{RSL})} = 1 - \frac{var(\mathrm{RSL} - \eta_p - \eta_T - \eta_S)}{var(\mathrm{RSL})}, \tag{7}$$

while the variances explained by the contributions in equation (1) are

$$R_i^2 = 1 - \frac{var(\mathrm{RSL} - \eta_i)}{var(\mathrm{RSL})}. \tag{8}$$

However, as the $\eta_i$ are not independent

$$R^2 \neq \sum_i R_i^2, \tag{9}$$

and comparison of equation (8) with equation (7) shows that

$$R^2 = \sum_i \left( R_i^2 - \sum_{j \neq i} \frac{cov(\eta_i, \eta_j)}{var(\mathrm{RSL})} \right). \tag{10}$$

Thus, covariances between the predictors are important as they contribute to the explained variance.

[26] In addition to covariances, the observed RSL and its contributions were analyzed with respect to linear trends. To remove contributions from short-term variability and the seasonal cycle, trends were computed from data low passed with a 1 year running mean. Prior to filtering the data, gaps were filled using the seasonal cycle. After filtering, the gaps were reinserted and trends have been obtained by linear regression using least squares. The respective uncertainties are given by the 95% confidence intervals of the regression coefficients.

[27] To assess the trend of the residual sea level, that is the sea level that is not explained by vertical land uplift and changes in surface pressure and hydrography, the following linear model is assumed

$$\eta = \beta_0 + \beta_1 t + \beta_2(\eta_p + \eta_T + \eta_S) + \epsilon \tag{11}$$

$$\beta_1 = \beta_1^* - \mathrm{GIA}. \tag{12}$$

Here, $\eta$ is the observed RSL and $\beta_i$ are the coefficients obtained by regressing $\eta$ on time $t$ and the sum of the components, and minimizing the error term $\epsilon$ using the least squares method. As GIA represents a pure linear trend with a relatively large uncertainty, it is treated separately from the other components. In the above expressions, $\beta_0$ is the intercept of the model, and $\beta_2$ is a measure for how much of the variability of $\eta$ is explained by the sum of steric and barometric contributions and is close to 1 if those contributions account for most of the variability. $\beta_1$ represents a linear trend in RSL and includes vertical land uplift as well

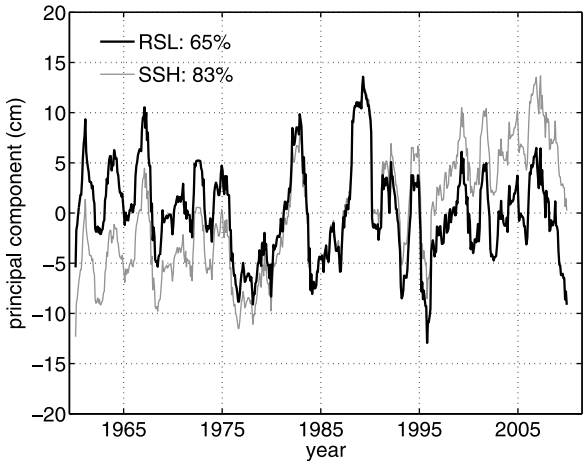


**Figure 2.** The leading mode of variability of observed RSL along the Norwegian coast (black), and the leading mode of SSH, i.e., RSL corrected for vertical land uplift (gray). Explained variances are 65% for RSL and 83% for SSH data.

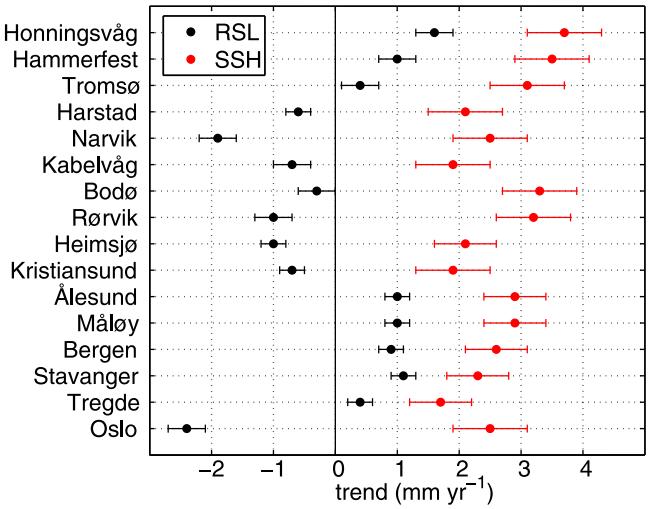


**Figure 3.** Trends of relative sea level (RSL, black) and sea surface height (SSH, red) from the period 1960–2010 in mm yr $^{-1}$ for tide gauges presented in Table 1.

as the residual (unexplained) trend, $\beta_1^*$. $\beta_1^*$ represents the trend in SSH and is obtained by $\beta_1^* = \beta_1 + \text{GIA}$. The respective uncertainties are computed from the square root of the summed square errors.

[28] To explore the common variability of all observations, we use empirical orthogonal function (EOF) analysis and present the corresponding principal components (PC). For vector fields such as surface wind, the components $u$ and $v$ are treated as two fields and the EOF analysis is performed on the joint matrix ($u$, $v$).

## 3. Results

### 3.1. Relative Sea Level and Sea Surface Height

[29] The RSL observations used in this study are spread along the Norwegian coast, thus spanning more than 10 latitudinal degrees. To extract the variability common to all stations, we perform an EOF analysis on the observations for the period 1960–2010. Gaps in the data are zero padded and all time series are low passed with a 1 year running mean filter prior to performing the analysis, in order to exclude contributions from the seasonal cycle. The leading mode of variability (Figure 2) explains 65% of the observed variance. The corresponding spatial pattern (not displayed) shows that this mode is most important in Oslo and north of Ålesund and less significant (but still positive) from Tregde to Måløy. The displayed RSL based on the first EOF is dominated by large interannual variability, particularly in the 1980s and early 1990s. A negative trend is seen in the first part of the record but it levels off sometime during the 1980s. The overall trend is $-0.4 \pm 0.3$ mm yr$^{-1}$ and therefore just significantly different from zero.

[30] To assess the effect of vertical land uplift given in Table 1, we compute linear trends from the observations of RSL for the period 1960–2010 (where available) and compare the results with trends corrected for land uplift, i.e., trends in SSH, in Figure 3. The RSL trends are spatially not uniform along the coast of Norway. They are positive from Tregde to Ålesund and north of Harstad, and negative or close to zero elsewhere. At Oslo, RSL is sinking at a rate of 2.5 mm yr$^{-1}$. After correcting for vertical land uplift, the trends are significantly larger and positive at all stations (>1.7 mm yr$^{-1}$, with a mean value of 2.6 mm yr$^{-1}$). Thus, vertical land uplift substantially weakens RSL rise along the Norwegian coast.

[31] The leading EOF mode of SSH (Figure 2) features a positive trend starting around 1985, indicating that rates of SSH rise were comparable to or exceed rates of vertical land uplift sometime during the 1980s. The linear trend in the SSH-EOF for the whole period is $2.9 \pm 0.3$ mm yr$^{-1}$, or 3.3 mm yr$^{-1}$ larger than the trend in RSL.

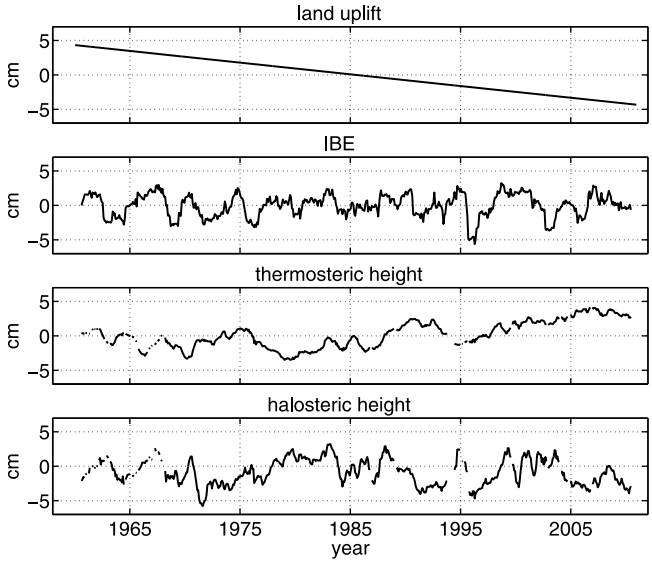


**Figure 4.** Contributions from land uplift, IBE, and thermosteric and halosteric heights to RSL variability in Bergen. For better visualization, the monthly time series have been low passed by applying a 1 year running mean.

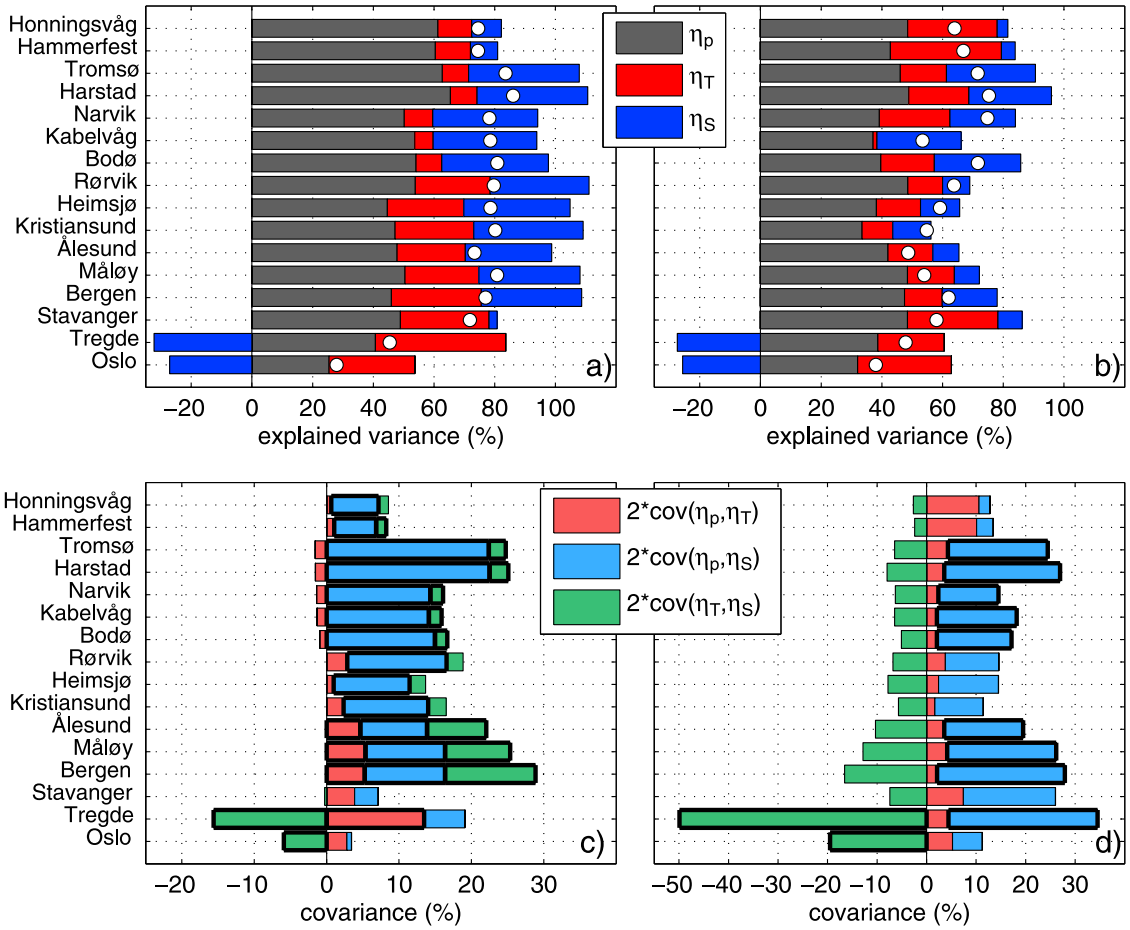


**Figure 5.** (top) Explained variances according to equations (7) and (8) for (a) high-pass-filtered and (b) low-pass-filtered data. Cutoff frequency is 1 year. Colored bars refer to the contributions and dots to their combination. (bottom) Covariances for (c) high-passed and (d) low-passed data. The covariances are normalized with var(RSL) and multiplied with a factor of 2 in accordance with equation (10). Thus, the difference between the sums of the bars in Figures 5a and 5c and Figures 5b and 5d equal the dots in Figures 5a and 5b, respectively. Covariances framed with a thick black line are statistically significant at the 99% confidence level.

### 3.2. Contributions to Relative Sea Level

[32] In this study, RSL at the tide gauge locations presented in Table 1 is reconstructed by computing and combining observed land uplift with SSH fluctuations induced by the IBE and thermosteric and halosteric height following equation (1). Figure 4 shows these contributions to the interannual (1 year running mean applied) RSL variability for Bergen. The IBE explains most of the variance (47%), while the thermosteric and halosteric components account for about 12% and 18%, respectively. Combined, they explain 62% of the observed interannual RSL variability in Bergen. Both the IBE and halosteric height are dominated by strong interannual variability with no obvious trends. In contrast, thermosteric height features low-frequency, decadal variation and a positive trend in the second half of the period.

[33] The explained variances of the single contributions as well as of their combination at all stations are summarized and presented in Figure 5. The analysis was performed for short-term and long-term variability, with a cutoff frequency of 1 year. Note that the trends are not included in the covariance analysis. Depending on the location, the reconstruction explains 28% to 86% of the observed intra-annual variability, and 38% to 75% of the observed interannual variability. The hydrographic station at Lista (Figure 1) may not be representative for the hydrography in the Oslofjord since it is remotely located. If Oslo is excluded, the minimum variance explained by our reconstruction is 45% on intra-annual and 48% on interannual time scales at Tregde.

[34] The sums of the explained variances of the contributions (color bars in Figures 5a and 5b) exceed the explained variance of the reconstructed RSL (dots) indicating covariability between the contributions (Figures 5c and 5d). Indeed, there are significant and positive covariances between IBE and thermosteric and halosteric height on intra-annual time scales. Covariances between IBE and halosteric height are strongest on intra-annual time scales, but are also present on interannual time scales. In addition, there is a tendency toward density compensation on longer time scales. The latter is, however, only significant at the two southernmost stations.

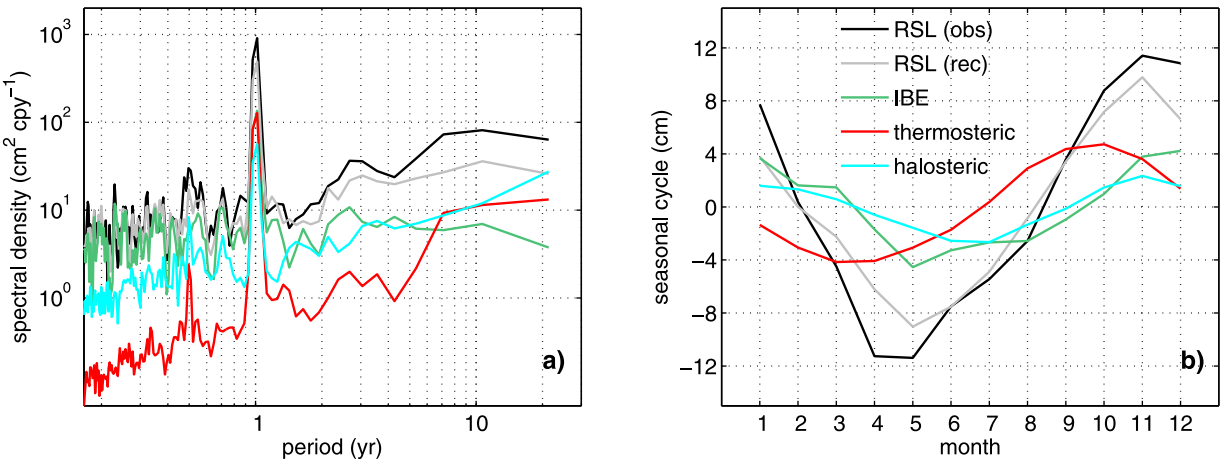


**Figure 6.** (a) Mean spectral density in cm$^2$ cpy$^{-1}$ (cycles per year) of observations (black), reconstruction (gray), and contributions from the IBE (green) and thermosteric (red) and halosteric (blue) heights. The data have been filtered with a 256 point Hanning window prior to computing the spectra. (b) Mean seasonal cycle.

[35] Except for the tide gauges in Oslo and Tregde, the contribution from the IBE is largest on both time scales. On intra-annual time scales, halosteric height equals or exceeds the contribution of thermosteric height hinting toward the importance of the relatively fresh water carried along the Norwegian coast by the Norwegian Coastal Current. On longer time scales, the relative contribution from halosteric height decreases. Apart from the southernmost stations Oslo and Tregde, both thermosteric and halosteric height contribute positively to the explained variance. Hence, there is in general no net density compensation present in the coastal water column. The explained variance of the reconstructed RSL decreases at interannual time scales (Figure 5a versus Figure 5b), indicating that other processes are more important on longer time scales.

[36] The explained variances for the unfiltered time series (not shown) are very similar to the explained variances for the high-pass-filtered time series in Figure 5a with maximum in Harstad (85%) and minimum in Oslo (30%).

[37] Due to the sparseness of the hydrographic stations as well as the rather coarse resolution of the gridded surface pressure field, only a few tide gauge stations are unique in terms of the chosen contributing factors. Based on the results in Figure 5 and the length and completeness of the available data record, Tregde, Stavanger, Bergen, Kristiansund, Tromsø and Hammerfest are selected for the following analysis.

[38] The temporal variability of observed RSL and its contributions is assessed by computing the respective spectra at each of the selected stations. The mean spectra are presented in Figure 6a. The IBE dominates on subseasonal time scales and is the least important contribution on decadal time scales. Except for a seasonal peak, its spectrum is white. The steric height spectra show increasing power with increasing periods. Common to all contributions is a distinct peak at the annual period. IBE and thermosteric height have on average the same amount of power in the seasonal cycle. However, the phase of the associated seasonal cycle varies (Figure 6b). While the IBE peaks in December, thermosteric height does so already in September/October. The contribution from halosteric height to the seasonal cycle is considerably smaller with a minimum centered around July and a maximum in November. The sum of all contributions has a mean seasonal cycle with an amplitude of about 9 cm and a minimum (maximum) in May (November) while the amplitude in the observations is 12 cm with minimum in April/May and maximum in November/December.

[39] Figure 7 presents the trends of the IBE and steric contributions. Comparison with rates of vertical land uplift (Table 1) shows that the uplift dominates the linear trend of the contributions. Vertical land uplift aside, the largest trend contribution is from the thermosteric component, ranging from 0.5 mm yr$^{-1}$ in Stavanger (Indre Utsira) to 1.0 mm yr$^{-1}$ in Kristiansund, where it has been computed over a shorter period, and Tregde. This result indicates a net warming of the water column along the entire Norwegian shelf. The halosteric contribution compensates with weak negative or close to zero long-term trends that correspond to a net salinification of the water column. The exception is

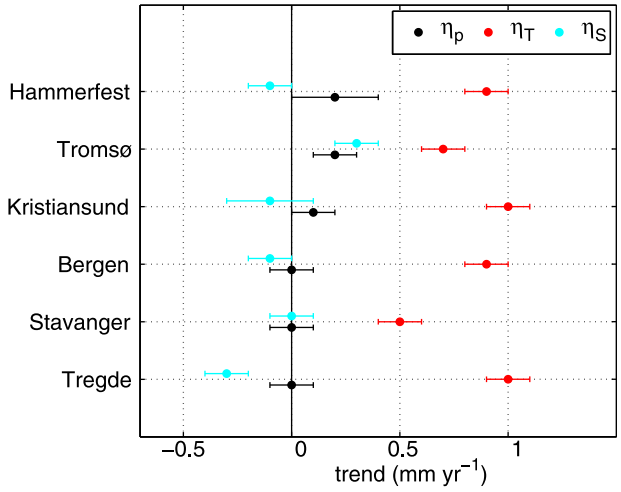


**Figure 7.** Observed trends of IBE (black) and thermosteric and halosteric heights (red and blue).

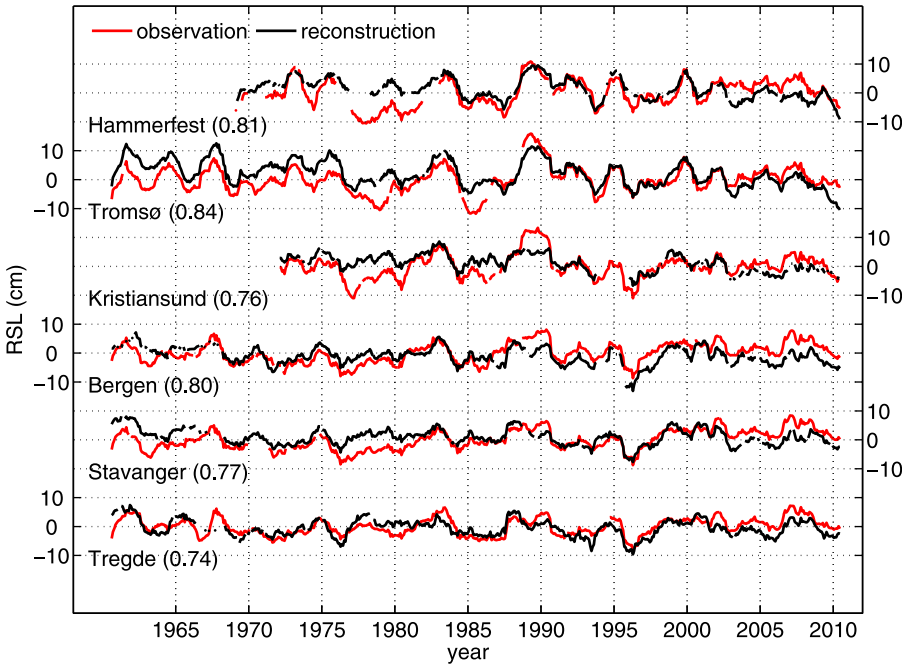


**Figure 8.** Observed (red) and reconstructed (black) RSL at selected stations. To improve the visualization and to emphasize interannual variability, the data has been low passed by using a 1 year running mean. Correlation coefficients between observations and reconstructions are presented.

Tromsø (Skrova) where freshwater appears to accumulate leading to a positive trend comparable to that of IBE. Trends due to long-term changes in surface pressure are insignificant except at the station in Tromsø where the IBE contributes positively to the trend.

### 3.3. Reconstruction and Residuals

[40] Figure 8 presents RSL observations at the selected stations together with their unique reconstructions. As there is no data available at the hydrographic stations in Ingøy and Bud prior to 1970 we cannot reconstruct RSL further back in time for Hammerfest and Kristiansund. Observed and reconstructed RSL agree well. The interannual variability is mostly captured by the reconstruction. There are however occasional deviations from the observations, e.g., in the late 80s from Bergen to Tromsø. As these excursions are present at several stations, it is unlikely that they are the result of erroneous observations but represent actual strong anomalies caused by other processes than those accounted for in this analysis.

[41] The residual trend, i.e., the trend that is not accounted for by our RSL reconstruction, and its uncertainty for the six selected stations are presented in Figure 9. The trend is positive for all stations and ranges from 1.3 mm $yr^{-1}$ at Tregde to 2.3 mm $yr^{-1}$ at Hammerfest (Table 2). These trends are comparable to or larger than the combined trend owing to pressure and steric changes (Figure 7). Evidently, additional processes contribute significantly to the observed long-term trends in RSL along the Norwegian coast.

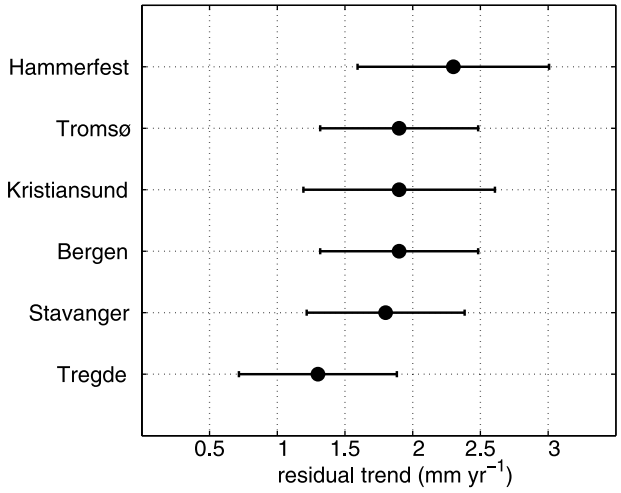


**Figure 9.** Residual trends, $\beta_1^*$, computed from equations (11) and (12) for the six selected stations.

## 4. Discussion

[42] We have estimated RSL variability along the Norwegian coast at various locations by accounting for vertical land uplift, atmospheric loading and steric contributions. The combination of these effects was compared to historical observations from tide gauges and we found that, depending on the location, our estimate explains 30–85% of

**Table 2.** Output of Model as Described by Equations (11) and (12)

| Station | $\beta_0$(mm) | $\beta_1$ (mm $yr^{-1}$) | $\beta_2$ | $\beta_1^*$ (mm $yr^{-1}$) |
|---|---|---|---|---|
| Hammerfest | 6934 | −0.2 | 1.1 | 2.3 ± 0.7 |
| Tromsø | 6958 | −0.8 | 1.0 | 1.9 ± 0.6 |
| Kristiansund | 7006 | −0.7 | 1.1 | 1.9 ± 0.7 |
| Bergen | 6949 | 0.2 | 0.9 | 1.9 ± 0.6 |
| Stavanger | 6925 | 0.6 | 1.0 | 1.8 ± 0.6 |
| Tregde | 7010 | 0 | 0.7 | 1.3 ± 0.6 |

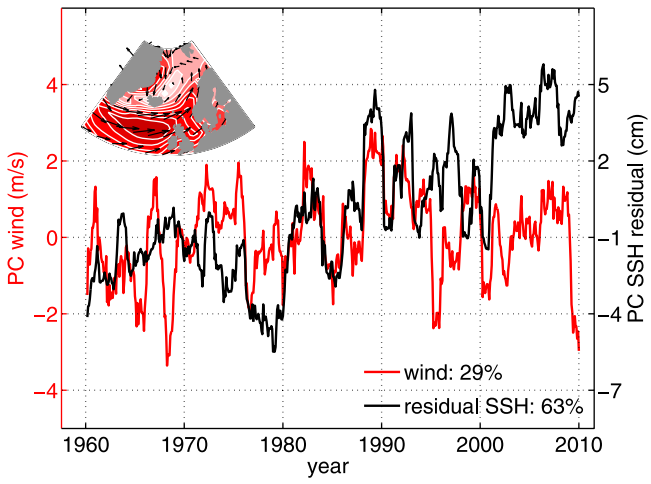


**Figure 10.** Principal components of the leading modes of NCEP wind over the northern North Atlantic (black) and residual sea level (red). For clarity, the principal components have been low passed with a 1 year running mean. Explained variances are indicated in the legend. The inset shows the normalized spatial wind pattern of the leading mode. Color coding is a measure for the strength of the wind amplitudes, ranging from 0 to 1 in intervals of 0.1.

the observed variability. On subdecadal time scales the bulk of the observed variability is explained by the IBE. In particular, IBE and halosteric height covary significantly, thus amplifying each other. Anomalously low sea surface pressure (positive IBE anomaly) is often related to more storms traveling into the area. Storms cause southwesterly wind anomalies that result in eastward propagation and subsequent downwelling of the fresh coastal water. These mechanisms are important on seasonal (Figures 5c and 6b) as well as interannual time scales (Figure 5d).

[43] Owing to strong land uplift, the trend in RSL is reduced substantially along the entire Norwegian coast. However, rates of sea level rise appear to be large enough to compensate for vertical land uplift, resulting in positive observed RSL trends along large portions of the coast. A similar result has been reported by *Rennie and Hansom* [2011] for the coast of Scotland where the land uplift is comparable to the uplift in southern and western Norway.

[44] The effect of thermal expansion is evident at all stations with trends of up to 1.0 mm $yr^{-1}$, thus dominating the trend budget compared to halosteric and surface pressure induced long-term variability. It is worth noting that the importance of the IBE trend increases toward higher latitudes. This is consistent with the reported decrease of surface pressure over the Arctic Ocean [*Walsh et al.*, 1996].

[45] The positive trend in the residual sea level indicates that the observed trend is substantially underestimated by our reconstruction. For the period 1960–2000, *Marcos and Tsimplis* [2007] found residual trends of 1.1 mm $yr^{-1}$ in the NE Atlantic and 1.3 mm $yr^{-1}$ in the North Sea. Those trends are comparable to the residual trends we found in Southern Norway. There are several factors not included into our analysis that may contribute to a rise in observed RSL.

[46] Changes in the circulation of the ocean contribute to sea level variability. Numerical models indicate that changes of the Atlantic Meridional Overturning circulation (AMOC) result in regional dynamic sea level changes [*Levermann et al.*, 2005; *Yin et al.*, 2010]. This effect may alter the influx of Atlantic Water to the Nordic seas in a warmer world, but it is likely small for the time period considered here. In addition, there is no observation-based evidence for long-term changes in AMOC, also indicating that the mentioned effect—for the present day climate—is small.

[47] Other forcing mechanisms for variability and trend that are worthwhile discussing, are (i) the dominant atmospheric pattern of variability in the Nordic seas favors southwesterly winds that, through Ekman transport, push water toward the coast; (ii) warming and/or freshening of the deep ocean within the Nordic seas result in ocean mass redistribution, moving water from the interior onto the shallow shelf areas; (iii) melting of land based ice redistributes water from land to the oceans while the opposite is true for the retainment of water, e.g., through storage. In the following sections these effects will be examined further.

### 4.1. Effect of Wind

[48] In order to assess the impact of wind on observed RSL, we perform an EOF analysis of the wind over the northern North Atlantic and Nordic seas, and compare it with the leading mode of the sea level residual (Figure 10). To also address the unexplained sea level variance on intra-annual time scales, monthly data are used. Surface wind is obtained from the NCEP-NCAR reanalysis [*Kalnay et al.*, 1996]. The following analysis has been duplicated using surface wind stress instead of wind, with essentially identical results (not shown).

[49] The leading mode of the wind field shows a pattern with strong westerlies over the Irminger Sea and winds parallel to a major portion of the northern European shelf. The corresponding principal component features seasonal (not shown), interannual as well as decadal variability. The latter includes a positive trend starting in the late 1960s persisting until the late 1980s. Since then, long-term fluctuations are moderate although superimposed by large interannual fluctuations. The correlation coefficients between PCs of wind and residual sea level are $r = 0.42$ on monthly time scales and $r = 0.19$ for data low passed with a 1 year running mean. The spectrum of the leading wind mode (Figure 11) has a peak at the annual period, suggesting that the part of the seasonal cycle not explained by our reconstruction (Figure 6) is caused by wind forcing. Indeed, the seasonal cycle of the leading wind mode has a strong minimum in May ($-3$ m $s^{-1}$) and a maximum in December and January (2 m $s^{-1}$) (not shown).

[50] In addition to the seasonal cycle, the spectra of leading modes of wind and sea level residual have increased power toward longer time scales (Figure 11), with the spectral density of the sea level residual exceeding those of the wind on the longest time scale. The positive trend in 1970–1990 is common to both time series, indicating that the rise in RSL during this period is partly wind driven. However, the observed RSL continues to rise although there is no apparent long-term trend in the wind forcing (Figure 10). The overall trend in wind is close to zero ($0.02 \pm 0.01$ m $s^{-1}$ $yr^{-1}$). This hints to other processes being responsible for the observed rise, in particular during the last decade.

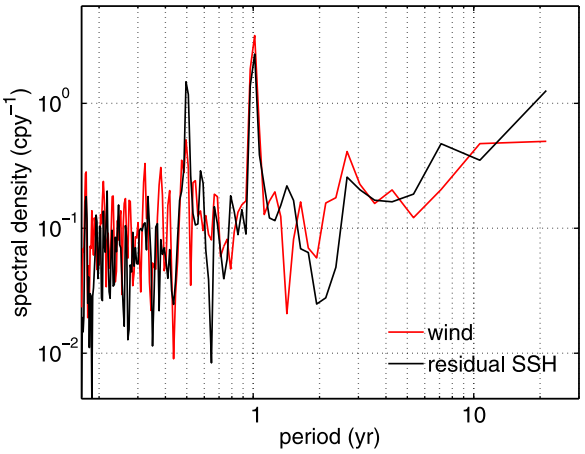


**Figure 11.** Spectral density in 1 cpy (cycles per year) of first principal component of wind (black) and sea level residual (red). The data have been standardized prior to computing the spectra. Spectra were computed using a 256 point fast Fourier transform with a Hanning window and 50% overlap.

### 4.2. Redistribution of Ocean Mass

[51] Steric sea level changes in the interior Nordic seas may affect SSH changes along the Norwegian coast through redistribution of ocean mass. In particular, changes in the thermohaline structure of the deep ocean generate horizontal pressure gradients at the surface with respect to the shallow shelf areas and ocean mass is transferred to balance the gradients [e.g., *Yin et al.*, 2010]. Warming of the deep abyss has been reported by *Østerhus and Gammelsrød* [1999] and attributed to the variability in the exchanges between the three deep basins of the Nordic seas. In addition, the warming signal observed in the upper ocean [*Holliday et al.*, 2008] may gradually penetrate into the deep ocean leading to even stronger warming there.

[52] Figure 12 shows changes in steric height computed in the 500–2000 m depth range at Ocean Weather Station Mike (OWSM, 66°N, 2°E) for the period 1960–2006. At these depths, the water masses are very cold and density follows mostly salinity. This translates to the steric height being governed by its halosteric component. However, thermosteric height tends to follow the steric height as well, i.e., as the water gets fresher it gets also warmer. Prior to the 1980s the steric height in the deep ocean features a weak negative trend but is mostly dominated by variability on shorter time scales. Around 1990, steric height increases abruptly at OWSM by roughly 1 cm within only 2 years. The fast increase is mostly accounted for by the halosteric component, i.e., freshening of the deep water whereas the thermosteric component increases more moderately. Steric height continues to increase steadily though at a lower rate than observed in 1990. The jump is due to warmer and fresher intermediate waters reaching OWSM and it is reasonable to assume that the filling up of the whole Nordic seas has been a gradual process since around 1980 [*Østerhus and Gammelsrød*, 1999]. The overall trend for the 1960–2006 period is 0.4 $\pm$ 0.1 mm yr$^{-1}$ while, for the period 1980–2006, the increase is 1.3 $\pm$ 0.1 mm yr$^{-1}$.

[53] As a result of increased SSH in the interior Nordic seas, ocean mass is transferred toward the shallow shelf, contributing to the observed sea level rise along the coast. The time scale of the adjustment of the sea surface is in the order of a few days (surface gravity waves). However, changes in the deep ocean alter the density structure of the water column (lifting isotherms etc). This leads to internal adjustment processes that take place on time scales of years to decades.

### 4.3. Mass-Exchange-Related Trends on the Norwegian Coast

[54] The world's ice sheets, glaciers and ice caps have been losing mass at an increasing rate over the last decades. As opposed to the other effects discussed in this paper, which redistribute mass inside the oceans, this adds mass to the oceans. As a direct result, the global sea level rises according to the mass received (eustatic sea level rise). However, the change in the earths gravitational field due of the loss of mass from the land sources, causes a redistribution of the sea level, in addition to the causes already discussed.

[55] In total, the mass loss from land ice has contributed to an eustatic sea level rise of 1.09 $\pm$ 0.26 mm yr$^{-1}$ in the period 1972–2008 [*Church et al.*, 2011]. This can be attributed to three main contributors: Greenland Ice Sheet (GIS) with 0.12 $\pm$ 0.17 mm yr$^{-1}$; Antarctic Ice Sheet (AIS) with 0.30 $\pm$ 0.20 mm yr$^{-1}$; and glaciers and ice caps (GIC) with 0.67 $\pm$ 0.03 mm yr$^{-1}$.

[56] When mass is lost from a region, such as an ice sheet or glacier, the (horizontal) gravitational pull from that region is weakened and water levels around the source sinks. This effect is not negligible. As explained by *Tamisiea et al.* [2003], the gravitational change results in a redistribution of global sea level equal to the exchanged mass multiplied by factors ranging from below zero to above one. These patterns are called fingerprints of the source in question, and reach around the globe with the strongest (diminishing) effect close to the source and above eustatic sea level rise in far away regions. There is also a smaller and slower but also

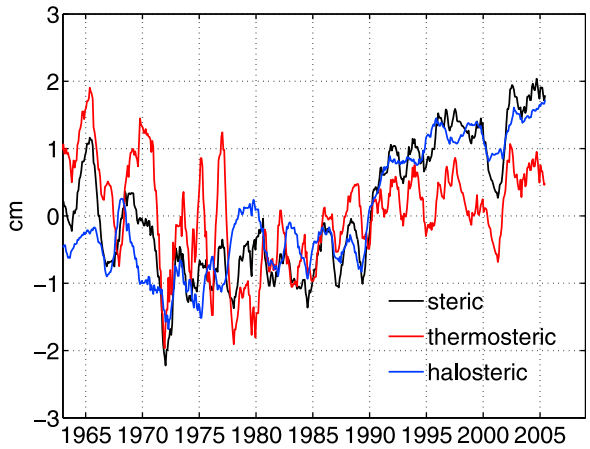


**Figure 12.** Steric height anomalies (black) computed between 500 and 2000 m from hydrographic profiles at OWSM. Thermosteric (red) and halosteric (blue) components are shown as well. The long-term mean was removed, and a 1 year running mean was applied.

global reaching crustal effect included in this. Factors for the Norwegian coast, related to the three mentioned ice sources, can be deduced from the fingerprint patterns provided by *Mitrovica et al.* [2001]: $f_{GIS} \approx 0.0$; $f_{AIS} \approx 1.0$; and $f_{GIC}$ ranges from 0.7 to 0.5 from southern to northern Norway. Due to the large uncertainties in both the mass loss estimates above and our residual trends (Figure 9), we will not be concerned with the spatial differences along the Norwegian coast and use a representative value of $f_{GIC} \approx 0.6$.

[57] The regional result of these three mass balance contributions can then be estimated as

$$\beta^*_{MB} = \Delta h_{GIS} \cdot f_{GIS} + \Delta h_{AIS} \cdot f_{AIS} + \Delta h_{GIC} \cdot f_{GIC}, \qquad (13)$$

where $\Delta h$ represent the three eustatic sea level trends given above.

[58] Error estimates for the fingerprint patterns are not provided in the literature, likely on the account of errors in the melt rates being much larger. And indeed, for our case, the large uncertainty in the AIS mass loss dominates the formal propagation of errors through (13), giving an error of 0.2 mm yr$^{-1}$ for $\beta^*_{MB}$. With respect to any influence from error in the fingerprint factors it would have to be as large as 0.2, which is unlikely judging from the level of detail in the fingerprint patterns presented in *Mitrovica et al.* [2001].

[59] The resulting mass loss contribution to sea level trend on the Norwegian coast for 1972–2008 is then $0.7 \pm 0.2$ mm yr$^{-1}$. This value is comparable with the independent (GRACE) gravity measurements of sea level change due to continental ice melt during 2003–2009 of $0.6 \pm 0.2$ mm yr$^{-1}$ for the same region [*Riva et al.*, 2010].

[60] In comparison with our residual trend of $1.9 \pm 0.6$ mm yr$^{-1}$ for the Bergen case, the loss of land-based ice explains about one third of the residual trend. Although this mass balance contribution to the Norwegian coast is for a different epoch than the 1960–2010 period used in the residual trend estimation herein (Figure 9), comparison is relevant.

[61] In addition to mass exchange from land based ice, effects such as retention of liquid water also comes into play, in the same manner, and the GRACE-measured total mass-exchange-related sea level trend for the Norwegian coast is $0.8 \pm 0.4$ mm yr$^{-1}$ during 2003–2009 [*Riva et al.*, 2010]. This is a more relevant number to compare our residual trend to, but valid only for a far shorter period.

## 5. Summary and Conclusion

[62] Natural and anthropogenically induced changes in RSL have strong implications for all coastal communities including those along the long coast of Norway. To project future changes in RSL it is essential to identify and quantify the different contributions to RSL variability and change.

[63] Subdecadal variability in RSL along the Norwegian coast has been examined by comparing tide gauge observations of RSL with hydrographic measurements (steric height), atmospheric surface pressure (IBE) as well as land uplift rates (GIA) for the period 1960–2010.

[64] It is found that these components account for 30–85% of the observed variability on monthly to interannual time scales, depending on location, and that the largest contribution to variability comes from IBE. For the steric effects, there are large regional differences along the coast.

[65] Linear trends in RSL are positive in southwestern and northern Norway. The most prominent contributions to the trend are the land uplift and a positive thermosteric contribution from a warming in the coastal waters (e.g., –1.7 and 0.9 mm yr$^{-1}$, respectively, for Bergen).

[66] The mentioned contributions explain less than half of the observed trend. One candidate for uncertainty is the vertical uplift rates. Other contributions not taken into account, but discussed, are wind effects, melting of land based ice as well as ocean mass redistribution due to hydrographic changes in the deep ocean. While being important on seasonal and interannual time scales, the effect of wind on the long-term trend appears to be minor. Likewise, little information about the melting ice sheets and glaciers is known prior to the advent of satellites, and modern estimates still vary largely. We estimate that melting of land-based ice has resulted in a rate of sea level rise of about $0.7 \pm 0.2$ mm yr$^{-1}$ along the Norwegian coast, corresponding to about one third of the unexplained trend. In addition, water masses in the deep Nordic seas appear to expand at a rate of $0.4 \pm 0.1$ mm yr$^{-1}$. It is however unclear, how this increase will affect RSL along the coast as it will also induce changes in the ocean circulation. Common to these additional effects is an increase since the 1980s, which is also seen in our unexplained residual series. While the large-scale winds do not contribute to a positive trend through the last 2 or 3 decades, the accelerating rates of loss of land-based ice may explain part of the remaining residual. In addition, changes in hydrology may contribute to the residual trend, but are also related to large uncertainties.

[67] Continued observations, in combination with a detailed numerical model, are likely needed to significantly improve our understanding of variations and changes in regional and local sea level.

[68] **Acknowledgments.** Hydrographic stations were obtained from the Institute of Marine Research, Bergen. We are grateful to Svein Østerhus for providing the data from the Ocean Weather Station Mike and to Laurent Bertino and David Stephenson for useful discussions. The comments of two anonymous reviewers helped to improve the quality of the paper. This work has received financial support from Bergen Kommune, the EU FP7 MONARCH-A project (grant 242446), and the Centre for Climate Dynamics at the Bjerknes Centre. This is contribution A396 from the Bjerknes Centre for Climate Research.

## References

Antonov, J. I., S. Levitus, and T. P. Boyer (2002), Steric sea level variations during 1957–1994: Importance of salinity, *J. Geophys. Res.*, *107*(C12), 8013, doi:10.1029/2001JC000964.

Cazenave, A., and W. Llovel (2010), Contemporary sea level rise, *Annu. Rev. Mar. Sci.*, *2*, 145–173.

Cazenave, A., A. Lombard, and W. Llovel (2008), Present-day sea level rise: A synthesis, *C. R. Geosci.*, *340*, 761–770.

Church, J. A., and N. J. White (2011), Sea-level rise from the late 19th to the early 21st century, *Surv. Geophys.*, *32*, 585–602, doi:10.1007/s10712-011-9119-1.

Church, J. A., N. J. White, R. Coleman, K. Lambeck, and J. X. Mitrovica (2004), Estimates of the regional distribution of sea level rise over the 1950–2000 period, *J. Clim.*, *17*, 2609–2625.

Church, J. A., et al. (2011), Revisiting the Earth's sea-level and energy budgets from 1961 to 2008, *Geophys. Res. Lett.*, *38*, L18601, doi:10.1029/2011GL048794.

Ekman, M. (1996), A consistent map of the postglacial uplift of Fennoscandia, *Terra Nova*, *8*, 158–165.

García-García, D., B. F. Chao, and J.-P. Boy (2010), Steric and mass-induced sea level variations in the Mediterranean Sea revisited, *J. Geophys. Res.*, *115*, C12016, doi:10.1029/2009JC005928.

Gill, A. E., and P. P. Niiler (1973), The theory of the seasonal variability in the ocean, *Deep Sea Res. Oceanogr. Abstr.*, *20*, 141–177.

Holliday, N. P., et al. (2008), Reversal of the 1960s to 1990s freshening trend in the northeast North Atlantic and Nordic Seas, *Geophys. Res. Lett.*, *35*, L03614, doi:10.1029/2007GL032675.

Hurrell, J. W. (1995), Decadal trends in the North Atlantic Oscillation: Regional temperatures and precipitation, *Science*, *269*(5224), 676–679.

Jevrejeva, S., J. C. Moore, P. L. Woodworth, and A. Grinsted (2005), Influence of large-scale atmospheric circulation on European sea level: Results based on the wavelet transform method, *Tellus, Ser. A*, *57*, 183–193.

Jevrejeva, S., A. Grinsted, J. C. Moore, and S. Holgate (2006), Nonlinear trends and multiyear cycles in sea level records, *J. Geophys. Res.*, *111*, C09012, doi:10.1029/2005JC003229.

Kalnay, E., et al. (1996), The NCEP/NCAR 40-year reanalysis project, *Bull. Am. Meteorol. Soc.*, *77*, 437–471.

Leuliette, E. W., and L. Miller (2009), Closing the sea level rise budget with altimetry, Argo, and GRACE, *Geophys. Res. Lett.*, *36*, L04608, doi:10.1029/2008GL036010.

Levermann, A., A. Griesel, M. Hofmann, M. Montoya, and S. Rahmstorf (2005), Dynamic sea level changes following changes in the thermohaline circulation, *Climate Dynamics*, *24*, 347–354.

Levitus, S., J. I. Antonov, T. P. Boyer, H. E. Garcia, and R. A. Locarnini (2005), Linear trends of zonally averaged thermosteric, halosteric, and total steric sea level for individual ocean basins and the world ocean, (1955–1959)–(1994–1998), *Geophys. Res. Lett.*, *32*, L16601, doi:10.1029/2005GL023761.

Llovel, W., B. Meyssignac, and A. Cazenave (2011), Steric sea level variations over 2004–2010 as a function of region and depth: Inference on the mass component variability in the North Atlantic Ocean, *Geophys. Res. Lett.*, *38*, L15608, doi:10.1029/2011GL047411.

Marcos, M., and M. N. Tsimplis (2007), Forcing of coastal sea level rise patterns in the North Atlantic and the Mediterranean Sea, *Geophys. Res. Lett.*, *34*, L18604, doi:10.1029/2007GL030641.

Marcos, M., F. M. Calafat, W. Llovel, D. Gomis, and B. Meyssignac (2011), Regional distribution of steric and mass contributions to sea level changes, *Global Planet. Change*, *76*, 206–218.

McClimans, T. A., B. O. Johannessen, and T. Jenserud (1999), Monitoring a shelf edge current using bottom pressures or coastal sea-level data, *Cont. Shelf Res.*, *19*, 1265–1283.

McDougall, T. J. (1987), Neutral surfaces, *J. Phys. Oceanogr.*, *17*, 1950–1964.

Meehl, G., et al. (2007), Global climate projections, in *Climate Change 2007: The Physical Science Basis*, edited by S. Solomon et al., pp. 847–940, Cambridge Univ. Press, Cambridge, U. K.

Meyssignac, B., F. Calafat, S. Somot, V. Rupolo, P. Stocchi, W. Llovel, and A. Cazenave (2011), Two-dimensional reconstruction of the Mediterranean sea level over 1970–2006 from tide gage data and regional ocean circulation model outputs, *Global Planet. Change*, *77*, 49–61.

Milne, G. A., J. L. Davis, J. X. Mitrovica, H. Scherneck, J. M. Johansson, M. Vermeer, and H. Koivula (2001), Space-geodetic constraints on glacial isostatic adjustment in Fennoscandia, *Science*, *291*(5512), 2381–2385.

Mitrovica, J. X., M. E. Tamisiea, J. L. Davis, and G. A. Milne (2001), Recent mass balance of polar ice sheets inferred from patterns of global sea-level change, *Nature*, *409*, 1026–1029.

Østerhus, S., and T. Gammelsrød (1999), The abyss of the Nordic seas is warming, *J. Clim.*, *12*, 3297–3304.

Pardaens, A., J. Gregory, and J. Lowe (2011), A model study of factors influencing projected changes in regional sea level over the twenty-first century, *Clim. Dyn.*, *36*, 2015–2033.

Pavlov, V. (2001), Seasonal and long-term sea level variability in the marginal seas of the Arctic Ocean, *Polar Res.*, *20*, 153–160.

Peltier, W. R. (2004), Global glacial isostasy and the surface of the ice-age Earth: The ICE-5G(VM2) model and GRACE, *Annu. Rev. Earth Planet. Sci.*, *32*, 111–149.

Proshutinsky, A., V. Pavlov, and R. H. Bourke (2001), Sea level rise in the Arctic Ocean, *Geophys. Res. Lett.*, *28*, 2237–2240, doi:10.1029/2000GL012760.

Proshutinsky, A., I. M. Ashik, E. N. Dvorkin, S. Häkkinen, R. A. Krishfield, and W. R. Peltier (2004), Secular sea level change in the Russian sector of the Arctic Ocean, *J. Geophys. Res.*, *109*, C03042, doi:10.1029/2003JC002007.

Proshutinsky, A., I. Ashik, S. Häkkinen, E. Hunke, R. Krishfield, M. Maltrud, W. Maslowski, and J. Zhang (2007), Sea level variability in the Arctic Ocean from AOMIP models, *J. Geophys. Res.*, *112*, C04S08, doi:10.1029/2006JC003916.

Rennie, A., and J. Hansom (2011), Sea level trend reversal: Land uplift outpaced by sea level rise on Scotland's coast, *Geomorphology*, *125*, 193–202.

Rignot, E., I. Velicogna, M. van den Broeke, A. Monaghan, and J. Lenaerts (2011), Acceleration of the contribution of the Greenland and Antarctic ice sheets to sea level rise, *Geophys. Res. Lett.*, *38*, L05503, doi:10.1029/2011GL046583.

Riva, R. E. M., J. L. Bamber, D. A. Lavallee, and B. Wouters (2010), Sea-level fingerprint of continental water and ice mass change from GRACE, *Geophys. Res. Lett.*, *37*, L19605, doi:10.1029/2010GL044770.

Siegismund, F., J. Johannessen, H. Drange, K. A. Mork, and A. Korablev (2007), Steric height variability in the Nordic seas, *J. Geophys. Res.*, *112*, C12010, doi:10.1029/2007JC004221.

Slangen, A. B. A., C. A. Katsman, R. S. W. van de Wal, L. L. A. Vermeersen, and R. E. M. Riva (2011), Towards regional projections of twenty-first century sea-level change based on IPCC SRES scenarios, *Clim. Dyn.*, *38*, 1191–1209.

Steele, M., and W. Ermold (2007), Steric sea level change in the Northern Seas, *J. Clim.*, *20*, 403–417.

Tamisiea, M. E., J. X. Mitrovica, J. L. Davis, and G. A. Milne (2003), Long wavelength sea level and solid surface perturbations driven by polar ice mass variations: Fingerprinting Greenland and Antarctic ice sheet flux, *Space Sci. Rev.*, *108*, 81–93.

Vestøl, O. (2006), Determination of postglacial land uplift in Fennoscandia from leveling, tide-gauges and continuous GPS stations using least squares collocation, *J. Geod.*, *80*, 248–258.

Wahl, T., J. Jensen, T. Frank, and I. Haigh (2011), Improved estimates of mean sea level changes in the German Bight over the last 166 years, *Ocean Dyn.*, *61*, 701–715.

Wakelin, S. L., P. L. Woodworth, R. A. Flather, and J. A. Williams (2003), Sea-level dependence on the NAO over the NW European continental shelf, *Geophys. Res. Lett.*, *30*(7), 1403, doi:10.1029/2003GL017041.

Walsh, J. E., W. L. Chapman, and T. L. Shy (1996), Recent decrease of sea level pressure in the central Arctic, *J. Clim.*, *9*, 480–486.

Weiss, J., J. Overpeck, and B. Strauss (2011), Implications of recent sea level rise science for low-elevation areas in coastal cities of the conterminous U.S.A., *Clim. Change*, *105*, 635–645.

Woodworth, P. L., and R. Player (2003), The permanent service for mean sea level: An update to the 21st century, *J. Coastal Res.*, *19*, 287–295.

Woodworth, P., W. Gehrels, and R. Nerem (2011a), Nineteenth and twentieth century changes in sea level, *Oceanography*, *24*, 80–93.

Woodworth, P., M. Menéndez, and W. Roland Gehrels (2011b), Evidence for century-timescale acceleration in mean sea levels and for recent changes in extreme sea levels, *Surv. Geophys.*, *32*, 603–618, doi:10.1007/s10712-011-9112-8.

Yin, J. J., M. E. Schlesinger, and R. J. Stouffer (2009), Model projections of rapid sea-level rise on the northeast coast of the United States, *Nature Geoscience*, *2*, 262–266.

Yin, J. J., S. M. Griffies, and R. J. Stouffer (2010), Spatial variability of sea level rise in twenty-first century projections, *J. Clim.*, *23*, 4585–4607.